Article

# Identifying Key Binding Interactions Between the Cardiac L-Type Calcium Channel and Calmodulin Using Molecular Dynamics Simulations

D'Artagnan Greene* and Yohannes Shiferaw

Read Online

ACCESS | Metrics & More | Article Recommendations | SI Supporting Information

**ABSTRACT:** Defects in the binding of the calcium sensing protein calmodulin (CaM) to the L-type calcium channel ($Ca_V1.2$) or to the ryanodine receptor type 2 (RyR2) can lead to dangerous cardiac arrhythmias with distinct phenotypes, such as long-QT syndrome (LQTS) and catecholaminergic ventricular tachycardia (CPVT). Certain CaM mutations lead to LQTS while other mutations lead to CPVT, but the mechanisms by which a specific mutation can lead to each disease phenotype are not well-understood. In this study, we use long, 2 $\mu$s molecular dynamics simulations and a multitrajectory approach to identify the key binding interactions between the IQ domain of $Ca_V1.2$ and CaM. Five key interactions are found between $Ca_V1.2$ and CaM in the C-lobe, 1 in the central linker, and 2 in the N-lobe. In addition, while 5 key interactions appear between residues 120−149 in the C-lobe of CaM when it interacts with $Ca_V1.2$, only 1 key interaction is found within this region of CaM when it interacts with the RyR2. We show that this difference in the distribution of key interactions correlates with the known distribution of CaM mutations that lead to LQTS or CPVT. This correlation suggests that a disruption of key binding interactions is a plausible mechanism that can lead to these two different disease phenotypes.
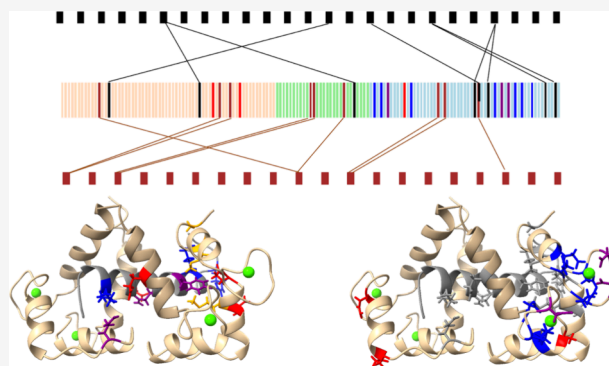
## INTRODUCTION

L-type calcium channels are found in many different cell types and play a role in a range of signaling processes. These include cell exo/endocytosis,[1] the immune response,[2] and neuronal communication and cell differentiation.[3,4] In the cardiac system, the opening of the voltage-gated L-type calcium channel ($Ca_V1.2$) on the outer cell membrane is responsible for producing an inward current that acts as an initiation signal in cardiac excitation-contraction coupling (ECC), which leads to a heartbeat.[5,6] Upon membrane depolarization, $Ca_V1.2$ briefly opens to allow calcium ions to flow from the extracellular space into the intracellular cytosol. This local increase in the cytosolic calcium concentration is large enough to activate nearby ryanodine receptor type 2 (RyR2) channels. RyR2 channels are embedded on the surface of an internal compartment called the sarcoplasmic reticulum (SR), which stores calcium ions. The binding of calcium induces the RyR2 channels to open and release calcium ions, leading to a much larger increase in the cytosolic calcium concentration. This process is known as calcium induced calcium release (CICR).[7] An elevated level of calcium in the cytosol triggers a calcium-dependent signaling cascade that ultimately culminates in a heartbeat.

After initiating the calcium signaling cascade, both $Ca_V1.2$ and RyR2 must close in the presence of an elevated cytosolic calcium concentration to terminate the initial signal and allow the cell to recover back to its original state. In $Ca_V1.2$, an important component of channel inactivation is calcium dependent inactivation (CDI).[8,9] In CDI, $Ca_V1.2$ interacts with the calcium sensing protein calmodulin (CaM), which mediates inactivation.[6,10] CaM is a ubiquitous calcium sensing protein that regulates numerous signaling processes involved in cell growth and cell communication.[11,12] For the case of the $Ca_V1.2$ channel, at resting calcium concentration levels, CaM binds to the $Ca_V1.2$ channel in a low-affinity, calcium-free form. However, as the calcium concentration in the cytoplasm rises, calcium binds to CaM, and this induces high-affinity calcium-dependent interactions that take place between CaM and $Ca_V1.2$. These interactions lead to inactivation of the channel.[8] In a similar way, calcium-bound CaM can inactivate the RyR2 at elevated calcium levels.[13]
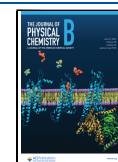
The structure of CaM consists of two lobes, an N-terminal lobe (N-lobe) and a C-terminal lobe (C-lobe), which are

connected to each other by a flexible linker. Each lobe consists of a pair of EF hand motifs which can bind to two calcium ions each for a total of four bound calcium ions when the calcium binding sites on CaM are fully saturated. The two lobes have a different affinity for calcium ions[14,15] with a $K_D$ of 0.1 $\mu$M in the high affinity C-lobe and a $K_D$ of 1 $\mu$M in the low affinity N-lobe. A widely accepted model describing CDI in Ca$_V$1.2 channels is that calcium binds to the C-lobe of CaM first to initiate CDI in Ca$_V$1.2 while the low affinity N-lobe of CaM binds to Ca$_V$1.2 at a later point as the calcium concentration further increases.[8,9]

The binding of calcium ions to CaM increases the affinity of CaM for specific target sequences of amino acids located within the Ca$_V$1.2 and RyR2 channels (Figure 1). Target
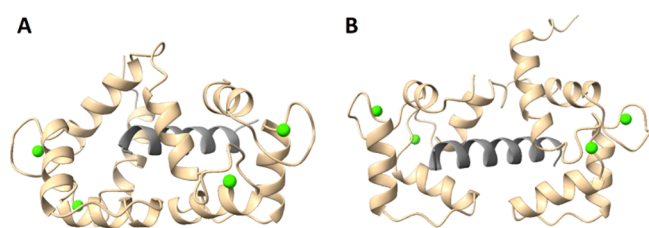


**Figure 1. Computational model of CaM bound to target sequence peptides for Ca$_V$1.2 and the RyR2.** (A) CaM (tan) is bound to the Ca$_V$1.2 target peptide (gray) while four calcium ions are bound to CaM (green). The N-terminal lobe of CaM and the N-terminal end of the Ca$_V$1.2 peptide are directed toward the left side of the image. (B) CaM (tan) is bound to the RyR2 target peptide (gray) while four calcium ions are bound to CaM (green). The C-terminal lobe of CaM and the N-terminal end of the RyR2 target peptide are directed toward the left side of the image. Both systems represent the initial structures just prior to running a MD simulation. The structures were derived from PDB IDs: 2F3Y and 6Y4O for the Ca$_V$1.2 and the RyR2, respectively.

sequence specificity is necessary to direct CaM to the proper cellular target at the proper time as calmodulin binding upregulates or downregulates many different proteins that are involved in ECC.[6,10] Calcium-bound CaM is known to bind to a distinct target sequence within Ca$_V$1.2 and a distinct target sequence within the RyR2. To initiate CDI, CaM binds to an IQ binding domain in Ca$_V$1.2 located within residues 1665−1685.[16] Available crystal structures indicate that CaM binds to the IQ domain in Ca$_V$1.2 in such a way that the N-lobe of CaM binds to the N-terminal end of the IQ target sequence while the C-lobe of CaM binds to the C-terminal end of the sequence (Figure 1A). Although it is generally agreed upon that the C-lobe of CaM binds to initiate CDI, several studies suggest that the N-lobe of CaM can also switch to bind to a different domain on Ca$_V$1.2.[17−20] For RyR2, the CaM binding sequence appears within residues 3584−3603. When CaM binds to the RyR2, the binding is opposite to that of Ca$_V$1.2 in the sense that the C-lobe of CaM binds to the N-terminal end of the RyR2 target sequence while the N-lobe of CaM binds to the C-terminal end of the sequence (Figure 1B). Defects in the binding of CaM to Ca$_V$1.2 or to the RyR2 can lead to dangerous cardiac arrythmias with distinct phenotypes such as long-QT syndrome (LQTS) and catecholaminergic ventricular tachycardia (CPVT).[5,21−26]

While defects in Ca$_V$1.2 and RyR2 target sequences can lead to disease phenotypes, it is also possible for disease phenotypes to appear due to defects in the structure of CaM.[21] Several

mutations in human CaM have been discovered that have been linked to different cardiac arrhythmia disease phenotypes[27] (Table 1). The vast majority of known CaM mutations

**Table 1. Known Human CaM Mutations and Disease Classifications**[a]

| Disease Phenotype | Mutation |
|---|---|
| CPVT | E46K, N54I, A103V |
| LQTS | D94A*, D96H*, D96V*, D96G*, N98I*, E105A*, D130A*, D130G*, D130V*, D132H*, D132V*, D132G*, D134H*, D134N*, Q136P, N138K, E141G*, E141V*, E141K* |
| CPVT and LQTS | N98S*, D132E*, D134N* |

[a]Mutations are separated by those that are associated with catecholaminergic polymorphic ventricular tachycardia (CPVT), with long-QT syndrome (LQTS), or with both disease phenotypes.[27] Mutations to residues that coordinate to calcium ions are indicated with an asterisk (*).

coordinate directly to calcium ions in EF hands III and IV in the C-lobe on CaM. These C-lobe mutations are commonly linked to LQTS, which is known to be associated with Ca$_V$1.2 dysfunction.[21,25] There are also two specific N-lobe mutations, E46K and N54I, that are not involved in calcium coordination but instead appear in a connecting loop between EF hands I and II in the N-lobe of CaM. These mutations, together with A103V, are associated with CPVT, which is known to be caused by defective association with the RyR2.[21,26] The three mutations N98S, D132E, and D134N are known to give rise to both disease phenotypes.

At present, it is not completely understood how certain CaM mutations can lead to the LQTS disease phenotype, associated with Ca$_V$1.2 dysfunction, while other mutations can lead to the CPVT disease phenotype, associated with RyR2 dysfunction. Knowledge about the binding specificity of CaM for the two main channels involved in ECC may be useful in designing a potential drug candidate that targets a specific cardiac disease by affecting only one of the two channels. To understand the differences in binding specificity for CaM binding to Ca$_V$1.2 and to the RyR2, we must identify and understand the key interactions taking place at the level of individual amino acid side chains between CaM and Ca$_V$1.2 and between CaM and the RyR2.[28−30]

One way to study key binding interactions between CaM and its binding targets in atomic detail is to use molecular dynamics (MD) simulations. In our previous study, we identified the key interactions involved in the binding of CaM to the RyR2.[31] In that study, we found that using both long MD simulations and a multitrajectory approach was necessary to deal with the structural heterogeneity observed between replicas at the end of our MD simulations. We showed that a small number of key interactions with high percent occupancy appeared in almost all of our replica systems despite the structural heterogeneity observed from replica to replica. These high percent occupancy interactions may be defined as those that fell within a 3.0 Å cutoff more than 20% of the time after a long equilibration of our MD simulations.

In this study, we identify key binding interactions between CaM and the IQ domain of Ca$_V$1.2. We show that 5 key interactions are found between Ca$_V$1.2 and CaM in the C-lobe, 1 in the central linker, and 2 in the N-lobe. Five key

**Table 2. Model System Nomenclature**[a]

| Model System Designation | Description |
|---|---|
| Ca$_V$1.2-WT* | 20 amino acid Ca$_V$1.2 wild type target peptide (KFYATFLIQEYFRKFKKRKEQ) bound to wild-type CaM (based on 2F3Y structure) |
| Ca$_V$1.2-Y1675H* | 20 amino acid Ca$_V$1.2-Y1675H mutant target peptide (KFYATFLIQEHFRKFKKRKEQ) bound to wild-type CaM (based on 2F3Y structure) |
| Ca$_V$1.1-WT* | 20 amino acid Ca$_V$1.1 wild type target peptide (KFYATFLIQEHFRKFMKRQEE)) bound to wild type CaM (based on 2F3Y structure) |
| Ca$_V$1.1-H1532Y* | 20 amino acid Ca$_V$1.1-H1532Y mutant target peptide (KFYATFLIQEYFRKFMKRQEE) bound to CaM (based on 2F3Y structure) |
| Ca$_V$1.2-WT*-Cap | 20 amino acid Ca$_V$1.2 target peptide (KFYATFLIQEYFRKFKKRKEQ) with an N-acetyl cap bound to wild type CaM (based on 2F3Y structure) |
| Ca$_V$1.2-WT (Ca$_V$1.2-CaM) | 26 amino acid Ca$_V$1.2 target peptide (EVTVGKFYATFLIQEYFRKFKKRKEQ) bound to wild type CaM (based on 2BE6 structure) |

[a]Model systems are designated according to the sequence of amino acids in the L-type channel Ca$_V$ target peptides. Systems listed with an * were based on the 2F3Y crystal structure, which was obtained from a 20 amino acid Ca$_V$1.2 target peptide consisting of the sequence: KFYATFLIQEYFRKFKKRKEQ, while the Ca$_V$1.2-WT (Ca$_V$1.2-CaM) system was based on the 2BE6 structure, which we truncated down to a 26 amino acid target peptide of sequence: EVTVGKFYATFLIQEYFRKFKKRKEQ.

interactions appear between residues 120−149 in the C-lobe of CaM when it interacts with Ca$_V$1.2, whereas only 1 key binding residue is found within this region of CaM when it interacts with the RyR2. We show that this distribution of key interactions correlates with the known distribution of CaM mutations that lead to LQTS or CPVT. This suggests that a disruption of key binding interactions due to a nearby mutation is a plausible mechanism that can lead to these two different disease phenotypes.

## ■ METHODS

**Preparation of L-type Channel Model Systems for MD Simulations.** To validate our computational model, we gathered the available experimental binding affinity data of the Ca$_V$1.2-CaM system from a study by Halling et al.[32] This study contained binding affinity data for CaM bound to the cardiac L-type calcium channel (Ca$_V$1.2) and the skeletal L-type calcium channel (Ca$_V$1.1).[32] The wild type structure of CaM bound to the Ca$_V$1.2 target peptide was provided by Fallon et al., and the file for this structure was downloaded from the RCSB protein data bank (PDB ID: 2F3Y).[33] The structure file was edited to contain only CaM, the four bound calcium ions, and the Ca$_V$1.2 target peptide; all of the other information in the original PDB file was removed. The program Modeller[34] (version 10.4) was used to model in missing residues that appeared within residues 2−149 on CaM, and we note that our CaM residues were numbered using the HGVS residue numbering nomenclature.[21] The Ca$_V$1.2 wild type (Ca$_V$-1.2-WT*) target peptide was taken to be 20 residues (1665− 1685) containing the amino acid sequence: KFYATFLIQ-EYFRKFKKRKEQ.

Modeller was also used to model in any missing residues and to introduce mutations into three other L-type model systems bound to wild type CaM that were present in the Halling study:[32] a Y1675H mutant variant (Ca$_V$1.2-Y1675H*) of the Ca$_V$1.2 target peptide (KFYATFLIQEHFRKFKKRKEQ), the Ca$_V$1.1 wild type (Ca$_V$1.1-WT*) target peptide (KFYA-TFLIQEHFRKFMKRQEE), and the H1532Y mutant variant (Ca$_V$1.1-H1532Y*) of the Ca$_V$1.1 target peptide (KFYA-TFLIQEYFRKFMKRQEE). For all four systems used in the method validation, we left the N-terminal and C-terminal ends of the Ca$_V$1.2 target peptide free in their charged forms, as this is assumed to be the peptide structure used in the binding affinity experiments in the Halling study. Beyond our method validation, we also studied two other Ca$_V$1.2 systems. The first was a model of the Ca$_V$1.2 wild type system based on the 2F3Y

crystal structure, where we inserted an acetyl cap onto the N-terminal end of the peptide. We refer to this system as Ca$_V$1.2-WT*-Cap. The purpose of Ca$_V$1.2-WT*-Cap was to check for the effect of removing a positively charged binding interaction from the N-terminal end of the Ca$_V$1.2-WT* peptide. In addition, we studied the Ca$_V$1.2-CaM wild type structure (PDB ID: 2BE6) that was provided by Van Petegem et al. in a separate study.[35] The 2BE6 structure had an extended Ca$_V$1.2 peptide, which contained 5 additional amino acids on the N-terminal end of the peptide. We trimmed the Ca$_V$1.2 peptide provided in the original 2BE6 structure file down to the 26 amino acid sequence (1660−1685): EVTVGKFYATFLI-QEYFRKFKKRKEQ. We prepared this system for MD in a fashion identical to what was described above for the other systems used in the method validation. A listing of all the model systems that we studied is provided in Table 2.

**MD Simulation Protocol.** The Amber 22 software suite was employed in all of our MD simulations.[36,37] In our previous study, we found that using long, 1 $\mu$s MD simulations and multiple replicas was necessary to analyze CaM binding interactions to the RyR2 channel.[31,38] In this study, we extended the total simulation run time to 2 $\mu$s and used 4 replicas for each of our model systems for a total of 24 systems and 48 $\mu$s of total run time. Each system was placed inside an isotropic OPC water box with an initial size of 89.947 × 89.947 × 89.947 Å$^3$. 21,945 water molecules were initially added to the box using tleap. 3D-RISM was used to determine the optimal number of solvent ions to neutralize our system with a target solvent concentration of 150 mM of NaCl; 123 water molecules were removed at random and replaced with solvent ions.[39] For the Ca$_V$1.2-WT* system, this turned out to be 67 Na$^+$ ions and 56 Cl$^-$ ions. For other systems, these ion numbers were adjusted if there was any change in the net charge of a particular system. For example, for the Ca$_V$1.1 wild type system, we used 70 Na$^+$ ions and 56 Cl$^-$ ions to neutralize our system since the Ca$_V$1.1 peptide has a lower net charge by −3 compared to the Ca$_V$1.2 peptide. For all ions, we used the Li Merz 12−6−4 ion parameters with the C4 correction term applied using parmed.[40,41]

To extend the simulation length, we employed hydrogen mass repartitioning (HMR)[42] to all of our model systems. This change allowed us to increase the time step in our simulations from 0.002 to 0.004 ps, which in turn increased our total simulation run time for each replica to 2 $\mu$s. For most MD simulations, the parameter and topology files were generated using standard residue types in tleap, and the Amber 19 force

field (ff19SB) was employed in all MD simulations. The one exception was the Ca$_V$1.2-WT*-Cap system. In this system, an acetyl cap was first added in place of a hydrogen atom on the N-terminal end of the target peptide. Following this change, the parameter and topology files were generated using tleap as before.

For each MD simulation, a minimization was performed using 1000 steps of steepest descent followed by 1000 steps of conjugate gradient. A nonbonded cutoff of 10.0 Å was specified, the SHAKE algorithm was used, and the residues in both CaM and the target peptide were restrained to their initial positions using a harmonic potential with a force constant of 2.0 kcal/mol. The calcium ions were left unrestrained to correct for any suboptimal positioning of the calcium ions in the original crystal structure file. The system was heated to 303 K under NVT conditions using a Langevin thermostat for 120 ps. This was followed by density equilibration in the NPT ensemble for an additional 120 ps using the Monte Carlo barostat with isotropic pressure scaling and a pressure relaxation time of 1.0 ps. After density equilibration, the restraints to CaM and the L-type target peptide were removed, and the pressure relaxation time was increased to 2.0 ps, while all other simulation settings were kept the same. The simulation was then extended to approximately 2 $\mu$s of total run time for each system.

**L-type-CaM Binding Free Energy Calculations.** To assess the overall binding strength of the L-type target peptide for CaM in a given replica system, we calculated the Molecular Mechanics Poisson−Boltzmann Surface Area (MMPBSA) and Molecular Mechanics Generalized Born Surface Area (MMGBSA)[43] binding free energies between the L-type target peptide and CaM over the last 100 ns of the 2 $\mu$s MD simulation for each replica system. We calculated the binding free energy using a frame sampled every 0.5 ns for a total of 200 frames used in our analysis. Owing to the rather high uncertainties in normal-mode analysis, the entropy contribution was neglected in our binding free energy calculations. We then averaged our results together to obtain an average binding free energy over this 100 ns time frame. The 100 ns sampling time frame used for our analysis was determined by analyzing the RMSD plots for all 16 replica systems in our method validation (see Figures S1−S4) to find an acceptable range toward the end of the simulations where all systems had reached an adequate level of equilibration. Using this 100 ns time frame, the standard error in the calculated MMPBSA binding free energy for each of the 24 replica systems that appear in this study was less than 2 kcal/mol (Table S1). To validate our model, we compared our calculated average binding free energies for the Ca$_v$1.2-WT*, Ca$_v$1.2-Y1675H*, Ca$_v$1.1-WT*, and Ca$_v$1.1-H1532Y* model systems with the experimental binding affinities reported in the study by Halling et al.[32] We obtained a high correlation with experimental binding affinities, which serves as an additional validation that the sampling window and approximations we made were appropriate for this project.

We also carried out binding free energy calculations in the same fashion for our two additional systems, Ca$_V$1.2-WT*-Cap and Ca$_V$1.2-CaM. In our MMGBSA calculations, igb was set to 2 to employ the Onufriev, Bashford, and Case (OBC) generalized Born model,[44] and the salt concentration or the ionic strength was set to 150 mM in both MMPBSA and MMGBSA calculations.

**L-type-CaM Key Interface Contact Calculations.** To locate the key interactions at the L-type-CaM interface for our model systems, we analyzed the last 100 ns (200 frames sampled at 0.5 ns intervals) of the 2 $\mu$s MD simulation for each of our model systems. To calculate the interface contacts, a distance-based cutoff was used, with a cutoff distance of 3.0 Å between heavy atoms. This distance was chosen to be close to the mean cutoff distance of hydrogen bond (H-bond) donor-acceptor distances in common protein secondary structures.[45] In our prior study,[31] we found that H-bonds that appear with a high percent occupancy colocalize with energy peaks in other interaction types such as nonpolar and electrostatic interactions. This allowed us to focus on using a simple distance-based cutoff corresponding to the average distance of the H-bond interactions to identify the key interaction sites in our system. In addition, we identified the key interactions while analyzing both the interaction energies and the percent occupancy of the interactions at each residue location. What we found is that the energy approach and the percent occupancy approach predict the same set of high percent occupancy key interaction locations and that either approach can be used to identify the key interaction locations in the system. In this study, we utilize high percent occupancy interactions to locate the key L-type CaM interactions so that we can compare them to the high percent occupancy interactions identified for the RyR2-CaM system in our prior study. We define high percent occupancy interactions in our present study as any interaction that appeared within a 3.0 Å cutoff more than 20% of the time over the last 100 ns of the 2 $\mu$s MD simulation. While this approach may not identify every important interaction taking place in the system and it does not compare the importance of each interaction to each other, the most stable key interactions with the highest percent occupancy can be identified using this approach.

A list of high percent occupancy interactions for each replica in each model system is available in Tables S4−S9. Note that we avoided double counting duplicate interactions between certain residues with multiple H-bond donors. For example, a glutamate interaction on CaM can have two oxygens interacting with the same residue on the L-type peptide, and this would show up twice in our raw percent occupancy calculations. In Tables S4−S9 and in all of the Figures and Tables that follow, we count this as only a single "unique" interaction and report the highest percent occupancy that was found for this interaction. The percent occupancy calculations were carried out using cpptraj in Amber 22.[46]

## RESULTS

**Binding Free Energy Calculations for the L-type-CaM Model Systems Correlate with Experimental Binding Affinities.** For our method validation, we compared our calculated average binding free energies for the Ca$_v$1.2-WT*, Ca$_v$1.2-Y1675H*, Ca$_v$1.1-WT*, and Ca$_v$1.1-H1532Y* model systems with the experimental binding affinities reported in the study by Halling et al.[32] using data sampled over the last 100 ns of each 2 $\mu$s MD trajectory. The RMSD plots for the 4 model systems in our method validation are provided in Figures S1−S4. The MMPBSA results for all four replicas of a given system are provided in Table S1, and these values were averaged together to obtain a single average binding free energy with a sample standard deviation to represent each model system, which is provided in Table S2. These average binding free energies were then compared to the experimental
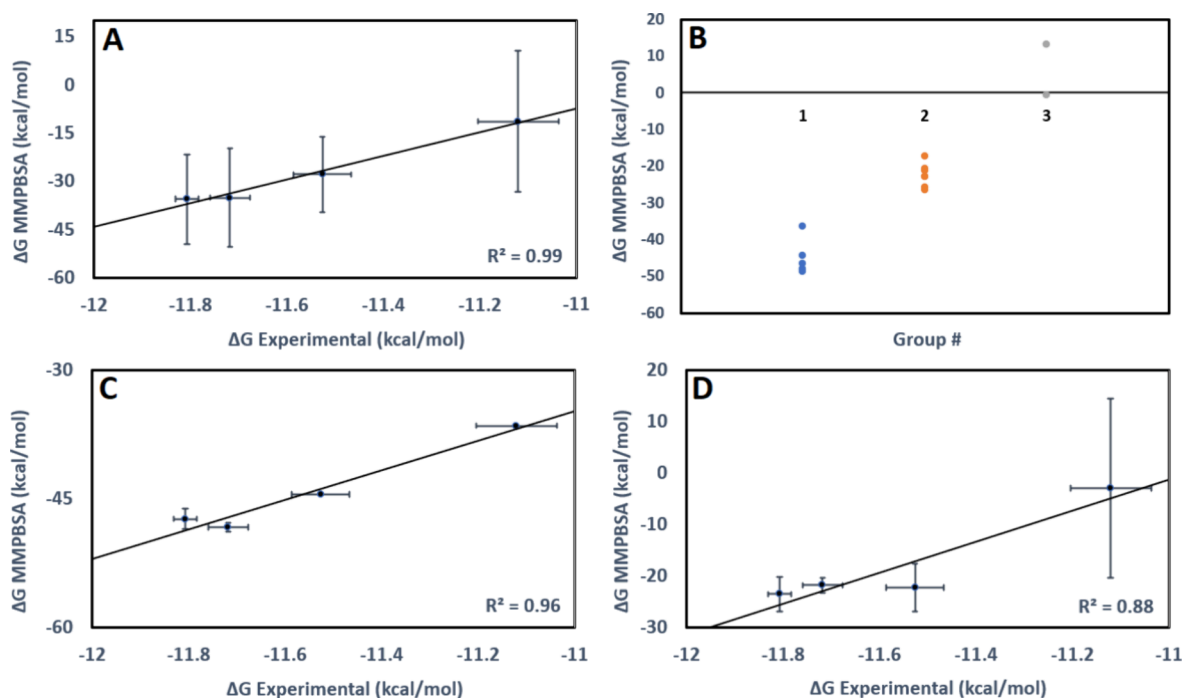
**Figure 2. MMPBSA method validation of L-type target peptide systems bound to CaM.** (A) MMPBSA method validation plot for L-type target peptides bound to wild type CaM. Each data point represents an average MMPBSA binding free energy obtained by averaging over 4 replica systems for each model system. A total of 16 2 $\mu$s MD simulations were used in our method validation. The binding free energy for each replica was an average of MMPBSA free energy calculations that were carried out every 0.5 ns over the last 100 ns of a 2 $\mu$s MD simulation. Experimental binding free energy values were obtained from binding affinity data in Halling et al.[32] (B) Strip plot showing the bimodal distribution of MMPBSA free energy values for Group 1 and Group 2/3 systems. (C) MMPBSA method validation plot using only Group 1 systems for L-type target peptides bound to wild type CaM. (D) MMPBSA method validation plot using Group 2/3 systems for L-type target peptides bound to wild type CaM. The binding free energy data used to generate this plot is available in the Supporting Information in Tables S1−S2.

binding free energy values obtained for these systems from the study by Halling et al.[32]

The result of our method validation is shown in Figure 2. The high $R^2$ values of 0.99 for MMPBSA and 0.91 for MMGBSA (Figure S5) indicate a strong correlation with the experimental binding free energy values. However, we note in Figure 2A that the standard deviation among our four replicas for any given system was large, on the order of 10−20 kcal/mol. Upon a closer examination of the free energy values for each individual replica for each model system, we observed a bimodal distribution of free energy values for 14 of the 16 replica systems (Figure 2B).

From a methodological standpoint, we note that this bimodal distribution of states would not have been observed if a single trajectory or structure was analyzed, and we note that these differences in the final state of each replica became apparent after each replica had time to equilibrate via the 2 $\mu$s of total simulation run time (Figures S1−S4). The importance of using multiple trajectories in free energy calculations in order to average over different states such as this was described rigorously in a study by Knapp et al.[38] Indeed, the high correlation for our MMPBSA and MMGBSA calculations would not have been observed unless a multitrajectory analysis that averaged over separate states was employed as suggested by Knapp et al.[38]

To uncover the source of this bimodal distribution of our free energy values in Figure 2B, we show the calculated binding free energies on a replica-by-replica basis in Figure 3A. We see that across all 16 2 $\mu$s MD simulations, 14 out of the 16 replica systems can be separated into two groups where Group 1 has

binding affinities less than −30 kcal/mol, while Group 2 has binding affinities between −10 and −30 kcal/mol. There are two exceptions in the Ca$_V$1.1-WT* system, where two of the replica systems are far above the −10 kcal/mol threshold, indicating that these two replica systems are far less stable than the majority of our other systems. We classify these two Ca$_V$1.1-WT* replica systems as Group 3. In Figure 2C,D, we redid our method validation using only Group 1 (Figure 2C) and Group 2/3 (Figure 2D). We note that we retain a high correlation with experimental binding affinities in both subsets while the standard deviation for each system decreases to between 0 and 5 kcal/mol for all systems except for the Ca$_V$1.1-WT* system, which is due to the two unstable Group 3 systems in its replica set. We will see later that the bimodal separation in free energy values between Group 1 and Group 2 systems is not arbitrary but can be narrowed down to the appearance of a specific key binding interaction that is present in all Group 1 systems but is not present in Group 2 and Group 3 systems.

**High Percent Occupancy Interactions Reveal Key Interaction Hotspots between the L-type Target Peptides and CaM.** Using the group designations for our 16 model systems, we can identify the key high percent occupancy interactions between the L-type target peptide and CaM to uncover the differences between the Group 1, 2, and 3 systems. The number of unique high percent occupancy interactions for each replica system in our method validation is shown in Figure 3B. Using the data in Figure 3B, the average number of high percent occupancy interactions over all 4 replicas for each system was calculated, and the results of this
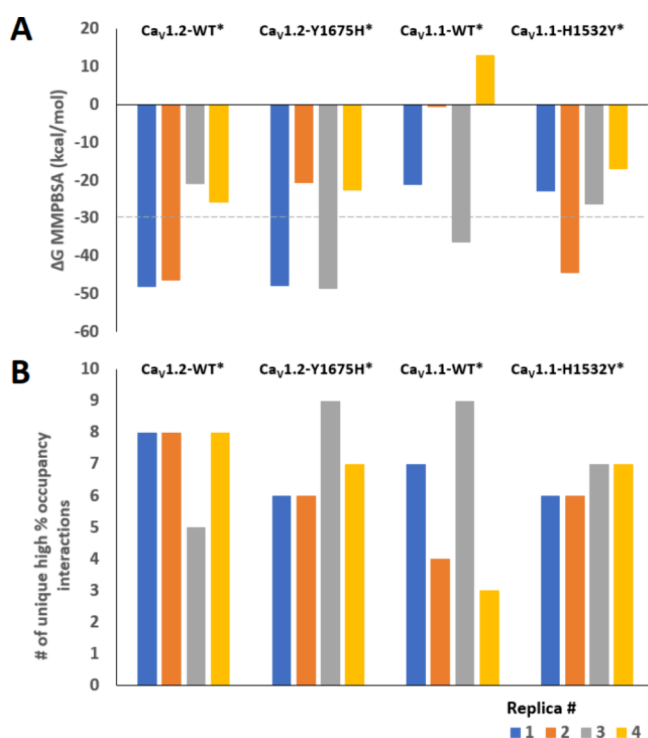
Figure 3. MMPBSA binding free energy values and the number of unique high percent occupancy interactions for each individual replica system in our method validation. (A) MMPBSA binding free energy values are provided for each of the four replicas in each of the four model systems used to calculate an average binding free energy in our method validation (Figure 2). A dividing line at −30 kcal/mol is provided to separate Group 1 systems with <30 kcal/mol from Group 2 and Group 3 systems with > −30 kcal/mol. (B) The number of unique high percent occupancy interactions identified per replica that was used in our method validation. High percent occupancy interactions are identified as unique interactions having a percent occupancy of 20% or greater over the last 100 ns of the MD simulation for each system. A listing of each individual binding free energy used to generate (A) is available in Table S1, while a listing of each individual high percent occupancy interaction used to generate (B) is available in Tables S4−S7.

calculation are provided in Table S3. The average number of high percent occupancy interactions is 7.25 for $Ca_V1.2$-WT*, 7 for $Ca_V1.2$-Y1675H*, 5.75 for $Ca_V1.1$-WT*, and 6.5 for $Ca_V1.1$-H1532Y*. This is in agreement with the rank order of our MMPBSA calculations in Figure 2A, which gave average values of −35.4 kcal/mol for $Ca_V1.2$-WT*, −35.0 kcal/mol for $Ca_V1.2$-Y1675H*, −11.3 kcal/mol for $Ca_V1.1$-WT*, and −27.7 kcal/mol for $Ca_V1.1$-H1532Y* (Table S2). In this way, the average number of high percent occupancy interactions correlates with the experimental rank order in terms of average binding free energies for our model systems.

While binding free energies and high percent occupancy interactions do correlate with each other on average, the deviations reported in Table S3 are large, and when we compare Figure 3A to Figure 3B we see that there are some cases where the two measures do not correlate. In Figure 3A, for example, replica 1 for $Ca_V1.2$-WT* has a binding free energy of −48 kcal/mol and 8 high percent occupancy interactions in Figure 3B, while replica 4 for $Ca_V1.2$-WT* has a binding free energy of −26 kcal/mol and also has 8 high percent occupancy interactions. This clearly indicates that the individual identity of the interactions, and not just their

absolute number, must also be taken into account to reliably distinguish between a Group 1 replica with a binding free energy less than −30 kcal/mol and a Group 2 replica with a binding free energy between −10 and −30 kcal/mol.

To examine the identity of each high percent occupancy interaction for Group 1−3 replicas, we calculated the average number of unique high percent occupancy interactions per replica at each residue position for both the L-type peptide (Figure 4A) and CaM (Figure 4B). Using $Ca_V1.2$ residue numbering (1665−1685), we can identify the positions along the L-type target peptide in Figure 4A starting with K1665 at the N-terminal end of the peptide and ending with Q1685 at the C-terminal end of the peptide. For CaM in Figure 4B, we number residues ranging from 2 to 149, which corresponds to using the HGVS nomenclature.[21]

In Figure 4A, we can identify K1665 at the N-terminal end of the L-type peptide as a high percent occupancy interaction in both Group 1 and 2 replica systems and, to a lesser extent, in Group 3 systems. F1666 appears as a high occupancy interaction location in Group 1 systems but does not appear in any Group 2 or 3 replica systems. The nearby A1668 is only observed in Group 1 and 3 replica systems. Q1673, Y1675, and K1678 are all observed in both Group 1 and 2 systems but are all more prominent in Group 2 systems. R1677 is a prominent contact in Group 1 and 3 systems but does not appear in any Group 2 replica systems. In its place, the neighboring K1678 is observed in Group 1 and 2 replica systems. K1680 and K1681 also appear in Group 1 and 2 replica systems. R1682 is a prominent contact in all three replica systems. Finally, K1683 appears only in Group 1 systems. As a qualitative check on our results, we note that Q1673, R1677, and R1682 are three highly conserved residues identified in a standard 1−5−10 IQ motif (IQXXXRXXXXR) shared by several different types of CaM-regulated proteins such as the L-type channel, Myosin, and Neuromodulin.[16,47] We also note that overall, several positively charged lysine (K) and arginine (R) residues on the L-type peptide form high occupancy interactions with CaM. This agrees well with mutation studies by Halling et al.[32] where it was observed that mutations at positions Y1675, K1680, and K1683 can all affect the binding affinity of the 20 amino acid (1665−1685) L-type target peptides for CaM.

In Figure 4B, we examine the number of high percent occupancy interactions at residue positions in CaM. Since CaM has a large number of residues, only residues with nonzero high percent occupancy interactions were included on the x-axis in Figure 4B. A prominent interaction involving residue E55 in the N-lobe of CaM is observed only in Group 1 systems. The second most prominent residue is E12 in the N-lobe of CaM, which is observed only in Group 1 and 3 systems. An N-lobe interaction is observed at residue E15 for the Group 1 and 2 systems. Residue L19 is only observed in Group 1 systems, while Q42 is only observed in Group 2 systems. While E85, E115, and E121 are more prominent Group 1 residues compared to Group 2, E88, E124, M125, E128, M145, and A148 are all observed more frequently in Group 2 systems than in Group 1 systems. We note that overall several negatively charged glutamate (E) residues on CaM form high occupancy interactions with complementary positively charged residues in the L-type peptide. In addition, nonpolar methionine (M) residues within the C-lobe of CaM assist in anchoring CaM to the L-type peptide.

The differences observed in Figure 4 reveal a subtle shift in binding for the Group 1 and Group 2 systems. Overall, we note
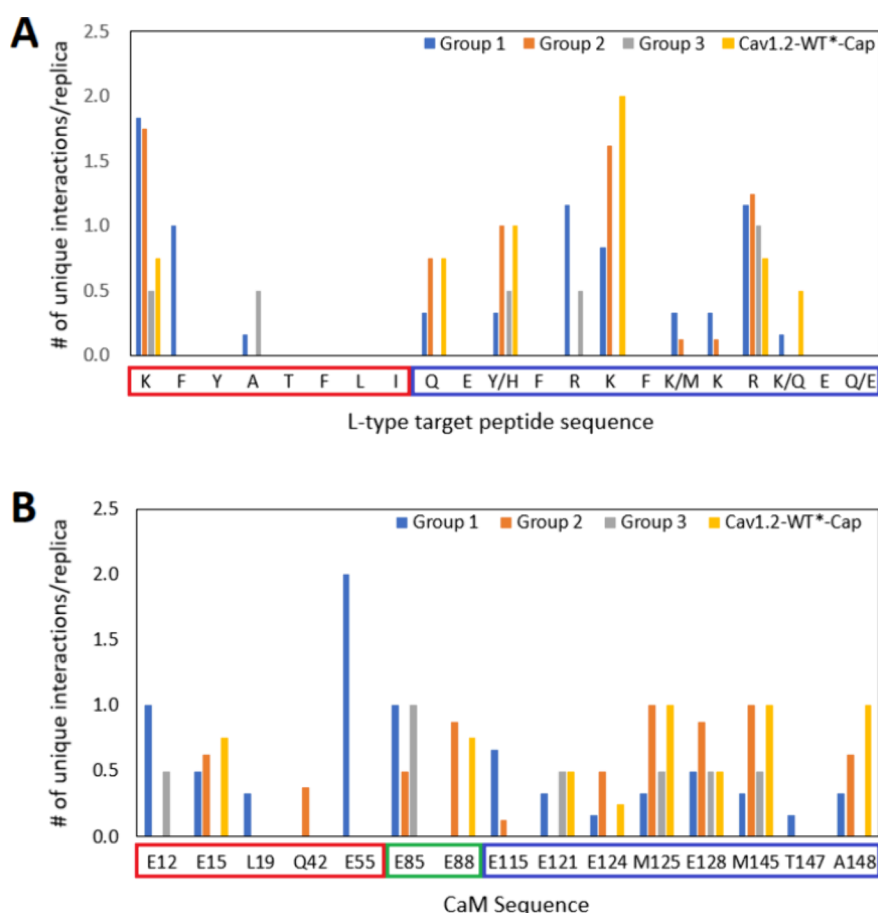
**Figure 4. Residues involved in unique high percent occupancy interactions for replica Groups 1−3 and Ca$_V$1.2-WT*-Cap.** The number of unique high percent occupancy interactions/replica for replica Groups 1−3 are given at each position along the L-type target peptide (K1665-Q1685 in Ca$_V$1.2) in (A) and at nonzero positions between residues 2−149 along CaM in (B). In (A), the N-terminal end of the target peptide (residues K1665−I1672) is highlighted in red on the *x*-axis while the C-terminal end of the target peptide (residues Q1673-Q1685) is highlighted in blue. In (B), the N-lobe of CaM (residues 1−64) is highlighted in red on the *x*-axis, the central linker (residues 65−92) is highlighted in green, while the C-lobe of CaM (residues 93−149) is highlighted in blue. Out of the 16 MD simulations used in our method validation, Group 1 replicas have a binding free energy of < −30 kca/mol, Group 2 replicas have a binding free energy between −10 and −30 kcal/mol, and Group 3 have binding free energies > −10 kcal/mol. Ca$_V$1.2-WT*-Cap is similar to the Ca$_V$1.2-WT* system except that an N-acetyl cap has been placed on K1665 to remove the N-terminal charge of the Ca$_V$1.2-WT* target peptide. A listing of each individual high percent occupancy interaction used to generate this figure is available in Tables S4−S8.

that more high percent occupancy interactions are observed in the N-lobe of CaM for Group 1 systems in comparison to Group 2 systems. The opposite trend is observed between residues 120−149 in the C-lobe of CaM when comparing Group 1 and Group 2 systems. Lower affinity Group 3 systems fall between these two extremes, displaying less prominent C-lobe interactions while also lacking the prominent K1665-E55 interaction found in Group 1 systems. The driving force behind this shift in binding between Group 1 and Group 2 systems appears to be the K1665-E55 interaction. The K1665-E55 interaction is the only key interaction present in every single Group 1 system, and it is also the only interaction absent in every single Group 2 and Group 3 system (Tables S4−S7). The observation that N-lobe contacts are more prevalent in Group 1 systems compared to Group 2, while the C-lobe contacts are significantly diminished, is also consistent with the N-lobe K1665-E55 interaction inducing a leftward shift in the binding of the L-type target peptide to CaM.

**An N-Terminal Interaction Can Stabilize Binding in Systems Based on the 2F3Y Crystal Structure.** Looking at these key interactions at the atomic level, we discovered an

anomaly with the K1665-E55 interaction in the Group 1 systems. While all of the other high percent occupancy interactions between the L-type peptide and CaM involved interactions between a side chain of a residue in the L-type peptide and a side chain of a residue in CaM, the K1665-E55 interaction involved an interaction with the free N-terminal end of the K1665 residue in the L-type peptide and the E55 side chain in CaM. This interaction is nonphysiological; it would not be present in the full-length L-type channel since K1665 at the N-terminal end of our target peptide would be connected to the next residue in the sequence in the full L-type channel. In the target peptide based on the 2F3Y model, there are two positive charges on the terminal residue K1665, one at the N-terminal end of the K1665 residue and one on the side chain of the K1665 residue. The positive charge on the N-terminal end would be neutralized as part of a backbone peptide bond in the full L-type channel. It can be confirmed visually in the original 2F3Y structure file provided in the study by Fallon et al. that the L-type peptide does not fully span the N-lobe in 2F3Y[33] (Figure 5A). Our high percent occupancy data indicate that this truncation facilitates an interaction
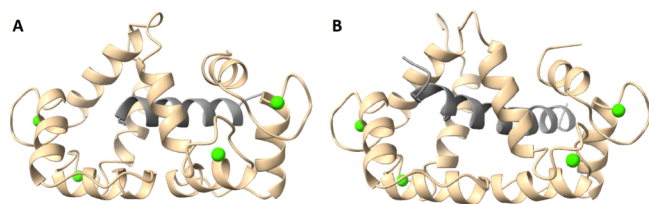
**Figure 5. Different lengths of Ca$_V$1.2 peptides in Ca$_V$1.2-CaM structures.** The Ca$_V$1.2-WT* model based on the 2F3Y structure is shown in (A) while the Ca$_V$1.2-WT (Ca$_V$1.2-CaM) model based on the 2BE6 structure is shown in (B). In (A) the 20 residue Ca$_V$1.2 peptide is displayed in gray while in (B) the 26 residue Ca$_V$1.2 peptide is displayed in gray. The N-terminal end of the peptide is directed to the left side of the image in both cases. CaM is shown in tan, and the N-terminal lobe of CaM is on the left side of the image in both cases. Calcium ions bound to CaM are displayed in green.

between K1665 at the free N-terminal end of the target peptide and residue E55 located within the N-lobe of CaM.

To test for the effect of removing this N-terminal interaction on the calculated binding affinity, we removed the positive charge on the N-terminal end of the L-type peptide in the Ca$_V$1.2-WT* system by adding an N-acetyl cap to it. We refer to the system where the N-terminal group has an acetyl cap attached to it as Ca$_V$1.2-WT-Cap*. For the Ca$_V$1.2-WT*-Cap system, we carried out additional MD simulations for 4 replica systems. The RMSD plots for this system are available in Figure S6, and the high percent occupancy interactions are listed in Table S8. MMPBSA/MMGBSA binding free energies were obtained by analyzing the last 100 ns of the MD simulation as before. It was found that the average MMPBSA binding free energy for Ca$_V$1.2-WT* at −35 kcal/mol dropped to −23 kcal/mol for Ca$_V$1.2-WT*-Cap. Although the standard deviations from the average value for all of our systems are large (Figure 2 and Tables S1 and S2), this result is at least consistent with the prediction that capping the N-terminal end in the Ca$_V$1.2-WT*-Cap system should lower the average free energy value substantially, and indeed we observe that the Ca$_V$1.2-WT-Cap* system has an average free energy value comparable to Group 2 systems that lack the K1665-E55 interaction.

Indeed, an examination of the high percent occupancy interactions in Table S8 and Figure 4A,B reveals that the K1665-E55 interaction is no longer observed for Ca$_V$1.2-WT*-Cap. In its place, a K1665-E88 interaction is observed where the side chain of residue K1665 is now participating in the interaction in place of the N-terminal group of K1665. Overall, the key interaction trends in the C-lobe in Ca$_V$1.2-WT*-Cap more closely resemble those seen in Group 2 systems compared to those in Group 1. This indicates that the removal of the K1665-E55 N-terminal interaction shifts the binding of the L-type peptide back toward the C-lobe of CaM in Ca$_V$1.2-WT*-Cap.

**Ca$_V$1.2-WT (2BE6) Restores Key Interactions between the Ca$_V$1.2 Target Peptide and the N-Lobe of CaM That Were Absent in Ca$_V$1.2-WT* (2F3Y).** In order to study the physiological interactions between CaM and the Ca$_V$1.2 peptide, we performed an analysis on the Ca$_V$1.2-CaM structure provided by Van Petegem et al.[35] (PDB ID: 2BE6). The 2BE6 structure features a Ca$_V$1.2 target peptide that is 5 residues longer on the N-terminal end of the target peptide, spanning the N-lobe of CaM (Figure 5B). The MMPBSA results for the Ca$_V$1.2-WT models based on 2F3Y

and 2BE6 are shown together in Figure 6A, and the data is available in Tables S1 and S2. On average, the MMPBSA
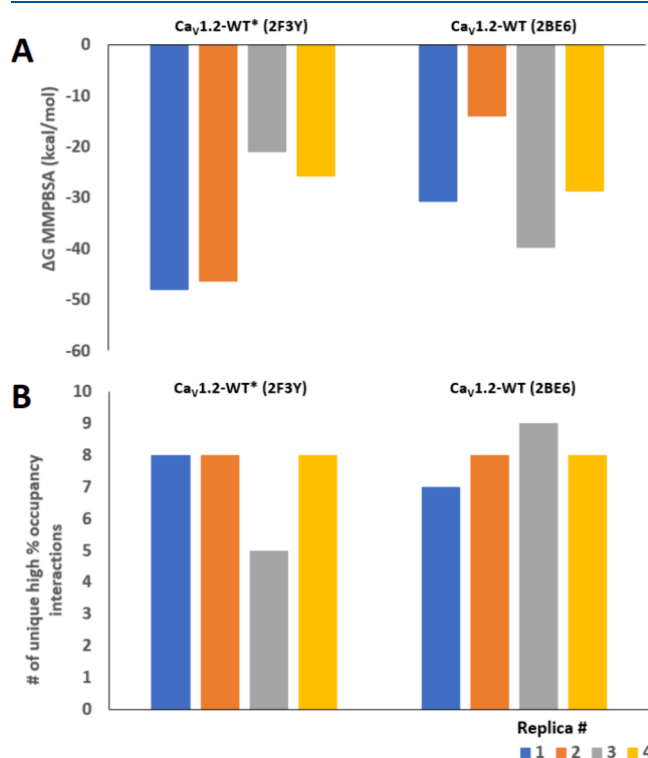


**Figure 6. MMPBSA binding free energy values and the number of unique high percent occupancy interactions for each individual replica system in our Ca$_V$1.2-WT models.** (A) MMPBSA binding free energy values for the Ca$_V$1.2-WT* replicas based on a 20 amino acid target peptide from the 2F3Y crystal structure and for the Ca$_V$1.2-WT replicas based on a 26 amino acid target peptide from the 2BE6 crystal structure. (B) The number of unique high percent occupancy interactions identified per replica for the Ca$_V$1.2-WT* replicas based on a 20 amino acid target peptide from the 2F3Y crystal structure and for the Ca$_V$1.2-WT replicas based on a 26 amino acid target peptide from the 2BE6 crystal structure. A listing of each individual binding free energy used to generate (A) is available in Table S1 while a listing of each individual high percent occupancy interaction used to generate (B) is available in Tables S4 and S9.

binding free energy for the Ca$_V$1.2-WT (2BE6) model is −28 kcal/mol, which is comparable to the −35 kcal/mol obtained for the Ca$_V$1.2-WT* (2F3Y) model. This is despite the lack of a K1665-E55 N-terminal interaction in the Ca$_V$1.2-WT (2BE6) system. The two models also have a similar number of high percent occupancy interactions, as shown in Figure 6B. The Ca$_V$1.2-WT* (2F3Y) model had an average of 7.25 high occupancy interactions while the Ca$_V$1.2-WT (2BE6) model had an average of 8 high occupancy interactions. A list of the high occupancy interactions for the Ca$_V$1.2-WT (2BE6) system is given in Table S9.

The average number of high percent occupancy interactions per replica for each residue location in Ca$_V$1.2-WT* (2F3Y) and Ca$_V$1.2-WT (2BE6) is given for the Ca$_V$1.2 peptide in Figure 7A and for CaM in Figure 7B. A comparison of the Ca$_V$1.2 target peptide interaction contacts in Figure 7A reveals that both Ca$_V$1.2-WT* (2F3Y) and Ca$_V$1.2-WT (2BE6) have very similar key hot spot residues. However, Figure 7B reveals that several changes take place in the binding of the Ca$_V$1.2 peptide to CaM when comparing the two systems. Residues
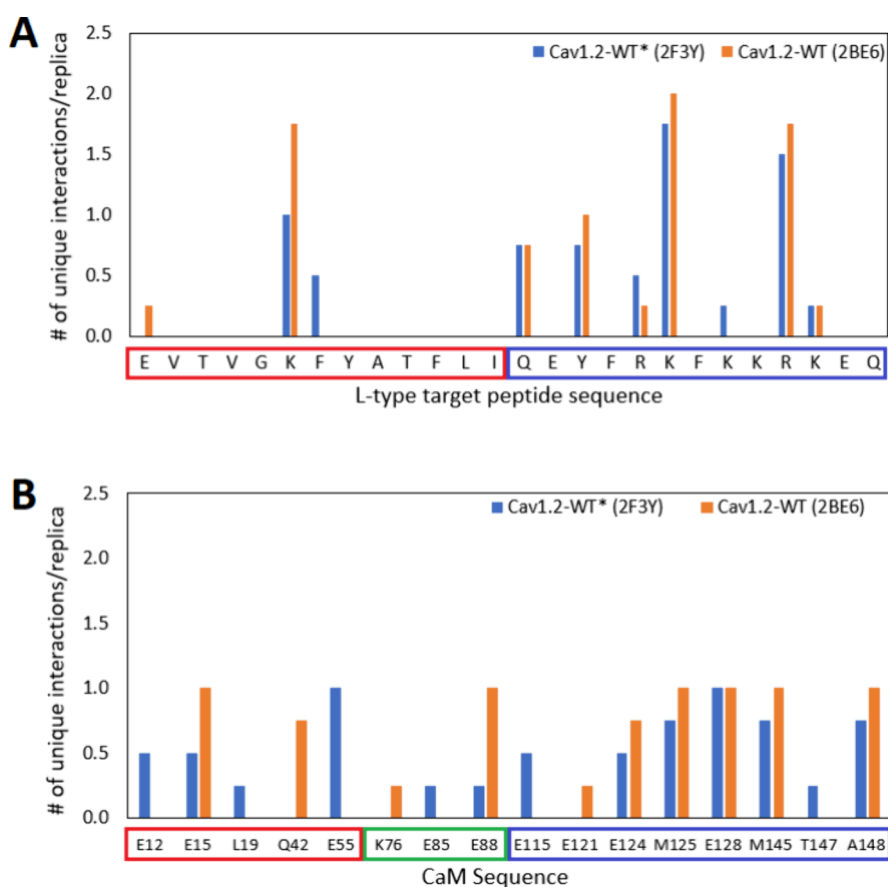
**Figure 7. Residues involved in unique high percent occupancy interactions in $Ca_V1.2$-WT target peptides and CaM.** The number of unique high percent occupancy interactions/replica for $Ca_V1.2$-WT systems are given at each position along the L-type target peptide (E1660-Q1685) in (A) and the nonzero positions between residues 2−149 along CaM in (B). In (A), the N-terminal end of the target peptide (residues E1660-I1672) is highlighted in red on the x-axis while the C-terminal end of the target peptide (residues Q1673-Q1685) is highlighted in blue. In (B), the N-lobe of CaM (residues 1−64) is highlighted in red on the x-axis, the central linker (residues 65−92) is highlighted in green, while the C-lobe of CaM (residues 93−149) is highlighted in blue. $Ca_V1.2$-WT* (2F3Y) has a 20 amino acid target peptide that is based on the 2F3Y crystal structure while $Ca_V1.2$-WT (2BE6) has a 26 amino acid target peptide that is based on the 2BE6 crystal structure. A listing of each individual high percent occupancy interaction used to generate this figure is available in Tables S4 and S9.

E15, Q42, K76, E88, E124, M125, M145, and A148 in CaM are more prominent binding partners in the $Ca_V1.2$-WT (2BE6) system while residues E12, L19, E55, E85, E115, and T147 are only present in the $Ca_V1.2$-WT* (2F3Y) system. In particular, we confirm that residue E55 on CaM no longer binds to the $Ca_V1.2$ peptide in any of our $Ca_V1.2$-WT (2BE6) replica systems. This is not surprising, as the N-terminal group on K1665 that was bound to residue E55 in $Ca_V1.2$-WT* (2F3Y) is no longer accessible for binding to residue 55 in the $Ca_V1.2$-WT (2BE6) system. Instead, in the $Ca_V1.2$-WT (2BE6) system, the side chain of the K1665 residue in the $Ca_V1.2$ target peptide is bound to residue Q42 on CaM.

The importance of the K1665-Q42 interaction to the binding free energy of the $Ca_v1.2$-WT (2BE6) system is readily apparent, as we did not observe this interaction in our second replica system of $Ca_V1.2$-WT (2BE6) while it was present in our other three $Ca_V1.2$-WT (2BE6) replica systems (Table S9). In the second replica system where this interaction did not appear, the binding free energy dropped to −14 kcal/mol, which was well-below the average of −28 kcal/mol taken over all four replica systems. Losing this interaction may also have some effect on the stability of the binding interface between $Ca_V1.2$ and CaM. In support of this notion, in Figure S8 we show that the RMSF noticeably rose in the central linker

region of CaM for replica 2 only. We also note that high occupancy interactions involving residues K76 and E121 on CaM appeared only in replica 2. The high occupancy interactions that were identified for the other three replica systems were very similar to one another as shown in Table S9.

Although we do not have an experimental binding affinity assay to directly validate the 2BE6 crystal structure that was used in our final model, the key interaction hot spots that we identified for the final model based on the 2BE6 crystal structure are the same as those identified in the 2F3Y crystal structure that was used for our method validation. These hotspots were additionally validated by comparisons to key residues identified in the experimental literature. Overall, the $Ca_V1.2$-WT (2BE6) system has a more complete peptide that spans the N-lobe of CaM in comparison to $Ca_V1.2$-WT* (2F3Y). From this point forward, we will use the $Ca_V1.2$-WT (2BE6) model exclusively in our analysis and refer to it as $Ca_V1.2$-CaM in the sections that follow.

**Key Binding Interactions in $Ca_V1.2$-CaM Reveal Three Distinct Binding Domains.** FIGURE 8 visualizes the key binding interactions for $Ca_V1.2$-CaM that were identified in Figure 7 for the $Ca_V1.2$-WT system. Since K76 and E121 were only observed in replica 2, and since replica 2 had a binding free energy much lower than the average for the other three
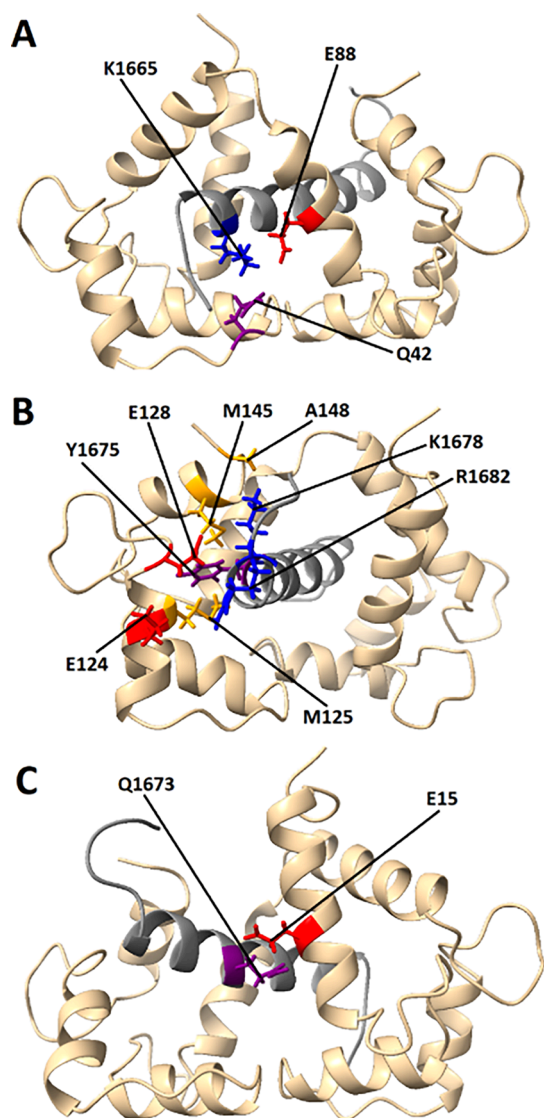
**Figure 8. Key binding interactions in the Ca$_V$1.2-CaM model.** The key high percent occupancy interactions in the Ca$_V$1.2-CaM model are shown. The 26 residue Ca$_V$1.2 target peptide is displayed in gray, and CaM is tan. Residues labeled within the sequence 1660−1685 are located on the Ca$_V$1.2 target peptide while residues labeled within the sequence 2−149 are located on CaM. In (A), the key interactions between the N-terminal end of the peptide (directed to the left) and the N-lobe of CaM (directed to the left) are shown; in (B), the key interactions between the C-terminal end of the peptide (directed to the left) and the C-lobe of CaM (directed to the left) are shown; and in (C), the key interaction between the C-terminal end of the peptide (directed to the left) and the N-lobe of CaM (directed to the right) is shown. The last frame of the 2 μs MD simulation for Ca$_V$1.2-CaM replica 1 is shown to illustrate the interactions.

replicas, we excluded these two interactions from Figure 8. The interactions in Figure 8 can be separated into three distinct binding domains: (1) the N-terminal end of the Ca$_V$1.2 target peptide binding to the N-lobe (residues 1−64) and central linker (residues 65−92) of CaM (Figure 8A), (2) the C-terminal end of the Ca$_V$1.2 target peptide binding to the C-lobe (residues 93−149) of CaM (Figure 8B), and (3) the Q in the IQ residue pair that is located in the middle of the Ca$_V$1.2 target peptide binding to the N-lobe of CaM (Figure 8C).

The first domain involves a single interaction between residue K1665 near the N-terminal end of the Ca$_V$1.2 target peptide and residues Q42 in the N-lobe of CaM and E88 in the central linker of CaM (Figure 8A). K1665 has a positively charged side chain that forms a salt bridge with E88 on one side and engages in a polar interaction with Q42 on its other side. This was the only key interaction we observed at the N-terminal end of the Ca$_V$1.2 target peptide. In terms of sequence, the next closest key interaction along the Ca$_V$1.2 target peptide involves residue Q1673, which is eight residues away in sequence.

The second domain involves the C-terminal end of the Ca$_V$1.2 target peptide binding to the C-lobe of CaM (Figure 8B). The interactions in this region are more numerous and structurally more complex, involving several residues on both the target peptide and the C-lobe of CaM. However, it can be broken down into essentially three separate interaction hotspots. The first is a hydrophobic interaction between the aromatic side chain on Y1675 on the target peptide and M125 on CaM. This interaction has by far the highest percent occupancy of all interactions observed in the Ca$_V$1.2-CaM system (Table S9), and it appears in a deep hydrophobic binding pocket near the center of the C-lobe. Two additional interactions involving positively charged residues K1678 and R1682 in the C-terminal end of the Ca$_V$1.2 target peptide interact with two residues apiece in the C-lobe of CaM. Residue R1682 forms a salt bridge with two negatively charged glutamate residues, E124 and E128, that appear on opposite sides of R1682 in three-dimensional space. Likewise, K1678 interacts with two nonpolar residues, M145 and A148, that are placed on opposite sides of K1678.

The third domain involves an interaction with Q1673 in the target peptide near the C-terminal end of the sequence and E15 on the far end of the N-lobe in CaM (Figure 8C). We note that this interaction appears on the opposite side of the structure from the interaction between K1665 and residues Q42 and E88. We also note that Q1673 is highly conserved, as it is the Q in the IQ residue pair that gives the series of IQ target sequences their name. In our method validation, Q1673 was not observed as a key interaction in our Ca$_v$1.1-WT* system, and Ca$_v$1.1-WT* had a much lower average binding free energy than the other systems (Figure 2 and Figure 3A). With the key interaction patterns for the Ca$_V$1.2-CaM system determined, we are now in a position to compare and contrast the key interactions observed in Ca$_V$1.2-CaM with those observed in RyR2-CaM from our prior study.[31]

## ■ DISCUSSION

**A Comparison of Key Interactions between Ca$_V$1.2-CaM and RyR2-CaM Reveals Differences in Binding Modes to Target Peptides.** Although mutations to CaM are implicated as being a central player in major cardiac diseases such as LQTS and CPVT, the mechanisms leading to one disease phenotype or the other are not completely understood. Such information must be made available before CaM can be targeted in pharmacological interventions in the cardiac system. Both the cardiac Ca$_V$1.2 channel and RyR2 play critical roles in ECC, and are both down regulated at the high calcium concentration levels in the cytosol that follow RyR2 channel opening. It was found that certain CaM mutations lead only to LQTS, others to CPVT, and some mutations lead to both disease phenotypes.[5] LQTS is primarily associated with Ca$_V$1.2 dysfunction while CPVT is primarily associated with
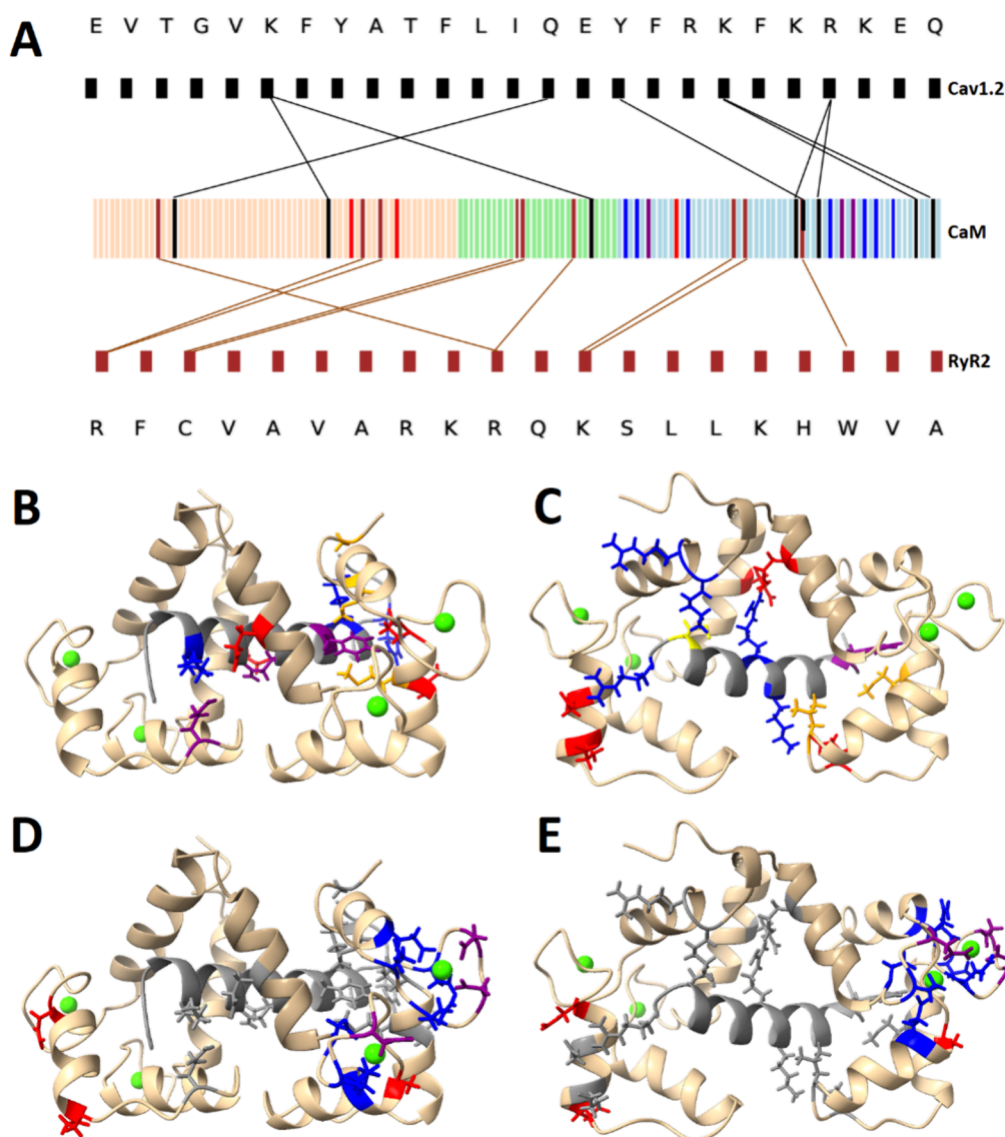
**Figure 9. Distribution of key interactions and LQTS/CPVT mutations in the Ca$_V$1.2-CaM and RyR2-CaM systems.** An interaction map of Ca$_V$1.2 (black) and RyR2 (maroon) binding to CaM is given in (A). Key interactions are shown as connections with black lines for Ca$_V$1.2 and brown lines for RyR2. On this map, LQTS mutations are indicated in blue, CPVT mutations are indicated in red, and LQTS/CPVT mutations are indicated in purple. The Ca$_V$1.2 target peptide (top) is orientated from the N-terminal on the left to the C-terminal on the right. CaM (middle) is oriented from the N-lobe on the left to the C-lobe on the right. The RyR2 target peptide (bottom) is oriented from the C-terminal on the left to the N-terminal on the right. Key interactions in the Ca$_V$1.2-CaM system are shown structurally in (B) and in the RyR2-CaM system in (C). In all structural images, the target peptide is colored gray, CaM is colored tan, the central linker in CaM (residues 65−92) is colored dark tan, and calcium ions are colored green. In (B) and (C), acidic residues are colored red, basic residues are colored blue, polar and aromatic residues are colored purple, nonpolar residues are colored orange, and cysteine is colored yellow. CPVT and LQTS mutations listed in Table 2 are mapped onto the Ca$_V$1.2-CaM system in (D) and onto the RyR2-CaM system in (E). In (D) and (E), mutations linked to CPVT are colored red, mutations linked to LQTS are colored blue, and mutations linked to both CPVT and LQTS are colored purple. The key interactions and target peptides from (B) and (C) are colored gray in (D) and (E). The structures shown were taken from the last frame of replica 1 in our MD simulations for both systems.

RyR2 dysfunction,[21] and this observation implies that at a structural level the binding of CaM to the RyR2 and Ca$_V$1.2 must be distinct in some way.

We had previously characterized the key binding interactions in the RyR2-CaM system[31] (Figure S9), and in this study we have determined the key binding interactions in the Ca$_V$1.2-CaM system (Figures 8 and S10). A comparison of our results reveals that certain principles in key interaction binding patterns are shared between RyR2 and Ca$_V$1.2, but there are also differences between the key interaction patterns that make the binding of CaM to Ca$_V$1.2 and RyR2 distinct. These

differences in key interactions can lead to a difference in binding specificity of CaM for Ca$_V$1.2 or RyR2 target peptides and provide a plausible explanation for why certain mutations are specific to LQTS or CPVT.

**Both Ca$_V$1.2 and the RyR2 Have Three Binding Domains, Use M125 on CaM as a Hydrophobic Anchor Residue, and Use Residue Triplets to Stabilize Interactions.** One similarity between binding of CaM to Ca$_V$1.2 and the RyR2 is that there are three distinct binding domains on CaM that can be identified. There is an N-lobe domain (residues 1−64), a C-lobe domain (residues 93−149), and a

central linker domain (residues 65−92) between these two lobes. With calcium fully bound, key interactions are observed in each of the three domains in both Ca$_V$1.2-CaM and RyR2-CaM (Figures S9−S10). Another similarity is that both structures feature a strong hydrophobic interaction in the C-lobe of CaM; the Y1675-M125 interaction in Ca$_V$1.2-CaM appears to be analogous to the hydrophobic anchor interaction that we observed between a tryptophan residue in the RyR2 peptide and residue M125 (W3586-M125) in CaM.[31] In both structures, this interaction has the highest percent occupancy of all of the key interactions that were identified in both systems. The Y1675-M125 interaction was identified previously as a key binding contact in the structural study by Fallon et al.,[33] and Y1675 mutants were studied in detail in the binding assay by Halling et al.[32]

Another common feature in Ca$_V$1.2-CaM and RyR2-CaM is the appearance of residue triplets to stabilize interactions. These triplets are arranged around basic residues, such as lysine and arginine. For example, in Ca$_V$1.2-CaM, residue R1682 appears to interact with nearby residues E124 and E128 which are placed on opposing sides of residue R1682 (Figure 8B). A similar situation is observed with residue K1678, which interacts with nearby residues M145 and A148 (Figure 8B). For residue K1665, a triplet is formed with residues Q42 and E88 (Figure 8A). Even though in this latter case residues Q42 and E88 are far apart sequence-wise, it can clearly be seen in Figure 8A that they appear on either side of K1665 in three-dimensional space. The last key interaction in the Ca$_V$1.2-CaM system is Q1673 to E15 which does not involve a basic residue. Taken together, the binding of CaM to Ca$_V$1.2 as seen in Figure 8 involves one major pairwise hydrophobic interaction, three basic residue triplet interactions, and one nonbasic residue pairwise interaction for a total of 5 key interaction hotspots.

When we compare this to the binding of RyR2 to CaM using Figure S9, we see that there are also residue triplets involving basic residues. In RyR2-CaM, R3594 forms a triplet with residues E85 and E12. As with Ca$_V$1.2-CaM, these residues are far apart in sequence but appear on adjacent sides of residue R3594 in three-dimensional space. Residue K3592 in RyR2 forms a triplet with nearby residues L113 and E115. Basic residues R75 and K76 appear to be competing with each other to form a triplet interaction with residue C3601. Finally, the basic residue R3603 forms a triplet with nearby acidic residues D51 and E48. Taken together, the binding of CaM to RyR2 involves one major hydrophobic interaction and four basic residue triplet interactions for a total of 5 key interaction hotspots. Overall, the total number of key interaction hotspots for CaM binding to the RyR2 and Ca$_V$1.2 appear to be about the same.

**Key Interactions Cluster in the C-Lobe in Ca$_V$1.2-CaM.** Both RyR2 and Ca$_V$1.2 have 5 interaction hotspots with CaM. However, while the total number of hotspots is the same in the two structures, they are seen to be distributed differently between the N- and C-lobes. An interaction map for Ca$_V$1.2 and RyR2 bound to CaM is provided in Figure 9A while the key interactions are mapped directly onto the structures in Figures 9B,C and S9−S10. In RyR2-CaM, there are 5 residues involved in high percent occupancy interactions in the N-lobe of CaM (E12, E48, D51, and E55), 3 residues in the central linker (R75, K76, and E85), and 3 residues in the C-lobe of CaM (L113, E115, and M125). In Ca$_V$1.2-CaM, there are 2 residues involved in high percent occupancy interactions in the

N-lobe of CaM (E15 and Q42), 1 residue in the central linker (E88), and 5 residues in the C-lobe of CaM (E124, M125, E128, M145, A148). A careful examination of these residue locations in Ca$_V$1.2-CaM reveals that 5 C-lobe residues in Ca$_V$1.2-CaM are located between CaM residues 120−149 while only 1 residue is located between CaM residues 120−149 in RyR2-CaM. Overall, key interactions are slightly more prevalent in the C-lobe in Ca$_V$1.2-CaM compared to RyR2-CaM, but key interactions are slightly more prominent in the N-lobe and central linker in RyR2-CaM compared to Ca$_V$1.2-CaM.

The observed differences in the spatial arrangement of these key interaction hotspots in Ca$_V$1.2-CaM and RyR2-CaM may be associated with differences in the physiological roles of the Ca$_V$1.2 and RyR2 channels with response to intracellular calcium levels. Since calcium binds with higher affinity to the C-lobe of CaM than to the N-lobe of CaM, stronger binding to the C-lobe would strengthen interactions between CaM and the target sequence of a channel at lower concentrations of calcium. On the other hand, calcium binding to the N-lobe of CaM would strengthen interactions occurring at higher concentrations of calcium. This shift in key interactions that we observe between Ca$_V$1.2 and RyR2 may therefore reflect a tuning of the channel response to calcium concentration. In Ca$_V$1.2-CaM, key interactions are clustered in the C-lobe of CaM, and we would expect Ca$_V$1.2-CaM to bind strongly to the C-lobe at low calcium concentrations. Since more RyR2-CaM key interactions appear in the N-lobe and central linker, we would expect that RyR2-CaM binding would not be fully optimized until higher calcium concentrations are reached. This would be essential to prevent RyR2 from closing prematurely, as it must open at low calcium concentration levels, remain open while the cytosolic concentration of calcium is increasing, and must close at high calcium concentration levels. Indeed, such a strategy for calmodulin binding to channel proteins was postulated by Cens et al. to explain the difference in calmodulin binding to Ca$_V$1.2 and Ca$_V$2.1.[8] In this case, CDI was observed in Ca$_V$1.2 due to a local increase in cytosolic calcium levels, and this was associated with the C-lobe of CaM binding to Ca$_V$1.2. In contrast, Ca$_V$2.1 channels only displayed CDI in response to global changes in calcium concentration, and this was associated with the N-lobe of CaM binding to Ca$_V$2.1.[8]

**Disease-Specific CaM Mutations Cluster around Key Interaction Hotspots within RyR2-CaM and Ca$_V$1.2-CaM.** In Figure 9A we have mapped the LQTS and CPVT mutations from Table 2 onto the key interaction map for Ca$_V$1.2-CaM and RyR2-CaM. In Figures 9D,E and S11−S12, we have mapped the mutation locations onto the structures for Ca$_V$1.2-CaM and RyR2-CaM. We see that LQTS mutations are clustered in the C-lobe of CaM, with 13/19 of the mutations that lead only to LQTS appearing between residues 120−149 at the end of the C-lobe. This parallels our key interaction map for Ca$_V$1.2-CaM, as five key interactions appear between residues 120−149 as shown in Figure 9A,D. For RyR2-CaM, we see that there is only one key interaction that appears between residues 120−149. Based on this observation, it seems reasonable to suggest that one factor that may cause these C-lobe mutations to be LQTS specific is that these mutations are in the proximity of many more potential key interactions in Ca$_V$1.2-CaM than for RyR2-CaM in this region of CaM. For RyR2-CaM, the only key interaction in the vicinity of these mutations is W3586-M125. The RyR2 might then be tolerant

to certain C-lobe mutations in CaM if a mutation does not abolish the W3586-M125 interaction. For example, Sondergaard et al. found that the F142 mutation impairs calcium binding to the C-lobe but does not affect calcium-dependent inhibition of the RyR2.[48] We note that two of the three mutation locations that lead to both LQTS and CPVT, D130 and D132, are located in proximity to the M125 residue, which is the only shared residue identified in key interactions for both Ca$_V$1.2-CaM and RyR2-CaM.

In general, the opposite occurs for the few known CPVT specific mutations. In Figure 9A,E we see that two out of the three CPVT mutation locations, N54 and E46, appear at the left end of the N-lobe. In RyR2-CaM, there is a key interaction involving residues E48 and D51 in CaM that appears directly adjacent to both of these mutation locations. The only residue that was observed near these residues in the Ca$_V$1.2-CaM system is Q42 (Figure 9A,D). Q42 interacts as part of a triplet with K1665 and E88 in Ca$_V$1.2; even if the Q42 interaction is disrupted, E88 may still interact with K1665 since E88 lies in the central linker, far from the CPVT mutation sites. As with C-lobe mutations and LQTS, mutations to the N-lobe are closer to key interaction hotspots for RyR2, which may help explain why these mutations lead to CPVT as opposed to LQTS.

While our results suggest a possible mechanism, whereby a local disruption of a key interaction in Ca$_V$1.2-CaM or RyR2-CaM via a CaM mutation may lead to either the LQTS or CPVT disease phenotype, we must point out that there are many other possible disease mechanisms that are outside the scope of this study, which may play a key role in influencing the overall disease phenotype. For instance, several studies[17−20] indicate that the N-lobe of CaM can bind to the N-terminal spatial calcium transforming element (NSCaTE) binding domain that is located some distance away from the IQ domain in Ca$_V$1.2 and Ca$_V$1.3. A pronounced CDI effect was found for the N-lobe in CaM binding to the NSCaTE domain in Ca$_V$1.3, and it was proposed that at high calcium concentrations, CaM can bind to both the NSCaTE domain and the IQ domain to create a bridge that solidifies closing of the L-type channel.[9,17] Some mutations can also affect the global conformation of CaM. For example, Wang et al.[49] demonstrated that the D130G mutation is severe enough to cause a complete separation of the EF hands within the C-lobe. This leads to complete unfolding of the C-lobe and the subsequent loss of calcium binding in EF hand 4.

In addition to variations in binding that may occur between the L-type channel and CaM, it is also possible that mutations can affect downstream targets of CaM differently. Prakash et al.[50] showed that the CPVT specific N54I and A103 V mutants interfere with calcium signaling via different mechanisms. While both mutants exhibited a decreased CaM binding affinity to the RyR2 in the presence of calcium, the two mutants were found to modulate CaM Kinase II differently, with N54I lowering phosphorylation activity by about 20% compared to the CaM wild type, while A103 V increased phosphorylation activity by about 60% compared to the CaM wild type. Theoharis et al.[51] showed that the type II IQ motif of the neuronal sodium voltage channel can lower the affinity of the C-lobe for CaM while IQ motifs in voltage-dependent Ca$^{2+}$ channels, kinases, and phosphatases have been shown to raise it. A mutation that affects the binding of calmodulin to CaM might therefore have different effects on different

channels, all of which contribute differently to the overall disease state.

At the whole cell, tissue, and organism levels, the downstream spatial and temporal effects of CaM mutations have been shown to be factors in disease phenotype. For instance, Jensen et al.[52] studied the effect of the CPVT specific N54I mutation and LQTS specific D96V mutation on *Caenorhabditis Elegans*. The authors observed alterations in two different rhythmic processes: pharynx pumping and the defecation motor program. The two mutations affect these two processes in distinctly different ways, and in addition to causing different cardiac arrhythmias, both mutations affected neuronal behavior differently, as well. Ultimately, the effects of CaM mutations on the binding of CaM to many different target proteins will be needed to understand the full impact a certain mutation can have on the overall disease phenotype in an organism.

## ■ CONCLUSION

To study the binding specificity between CaM and different target substrates, we used MD simulations to take into account the complex and dynamic interactions taking place between CaM and each target. Many existing approaches to identify binding hotspots are designed to use energy calculations on static structures, but here, we show that key interaction hotspot locations can also be identified as emerging from dynamic information taken from an ensemble of structures in a MD trajectory. Using long MD simulations and percent occupancy calculations to determine the key interaction sites can reveal time-dependent dynamic differences in the key interaction patterns between CaM and different cellular targets, such as Ca$_V$1.2 and the RyR2.

In this study, we determined the key interactions that take place when CaM binds to the IQ domain target sequence of the L-type Ca$_V$1.2 channel. We found 5 key interactions in the C-lobe of CaM between residues 120−149, which reflects the known importance of the C-lobe in CaM to induce CDI of Ca$_V$1.2. We also found 1 key interaction in the central linker and 2 in the N-lobe of CaM for a total of 8 key interactions between Ca$_V$1.2 and CaM.

When comparing our results to the key interactions for RyR2-CaM, we find 9 key interactions between the RyR2 and CaM. However, the spatial distribution of the key interactions is different in RyR2-CaM compared to Ca$_V$1.2-CaM. Three key interactions for RyR2-CaM are found in the N-lobe, in the central linker, and in the C-lobe of CaM, respectively. In contrast to CaV1.2-CaM, only one interaction is found between residues 120−149 in RyR2-CaM. The difference in the distribution of key interactions may play a role in differentiating binding of CaM to the two different channels, and it may lead to different disease phenotypes that are specific to each channel.

With regard to targeting CaM for future pharmaceutical interventions, quite a bit more must be known about how a given mutation can affect key interactions with CaM and many of its cellular targets before the overall effect of a drug on a given disease phenotype can be reliably predicted. Nevertheless, our results demonstrate that it is possible to design target sequence peptides that can compete with the wild type target sequence for binding to CaM. For example, the Ca$_V$1.2-WT* peptide based on the 20 amino acid target peptide demonstrated a rather pronounced and strong interaction between the N-terminal end of the target peptide and CaM.

This nonphysiological N-terminal interaction greatly affected the calculated binding free energy. At least in principle, a drug targeting Ca$_V$1.2 or CaM can be designed to exploit this higher affinity interaction. However, the effect of such a drug on many additional cellular targets, including RyR2, must be known in order to target the Ca$_V$1.2-CaM interaction without causing a myriad of side effects on other subcellular targets.

## ■ ASSOCIATED CONTENT

### Ⓢ Supporting Information

The Supporting Information is available free of charge at https://pubs.acs.org/doi/10.1021/acs.jpcb.4c02251.

RMSD plots for all 6 systems, MMGBSA method validation plot, RMSF plots for the Ca$_V$1.2-WT (2BE6) system, large key interaction images for the RyR2-CaM and Ca$_V$1.2-CaM systems, large mutation location images for the RyR2-CaM and Ca$_V$1.2-CaM systems, tables containing average MMPBSA and high percent occupancy results, all high percent occupancy interactions for all 6 systems (PDF)

## ■ AUTHOR INFORMATION

### Corresponding Author

D'Artagnan Greene − *Department of Physics and Astronomy, California State University Northridge, Northridge, California 91330-8268, United States of America;* ⊙ orcid.org/0000-0002-7836-9663; Email: dartagnan.greene@csun.edu

### Author

Yohannes Shiferaw − *Department of Physics and Astronomy, California State University Northridge, Northridge, California 91330-8268, United States of America*

Complete contact information is available at: https://pubs.acs.org/10.1021/acs.jpcb.4c02251

### Notes

The authors declare no competing financial interest.

## ■ ACKNOWLEDGMENTS

## ■ REFERENCES

(1) Nanclares, C.; Baraibar, A. M.; Gandia, L. L-type calcium channels in exocytosis and endocytosis of chromaffin cells. *Pflugers. Arch.* 2018, *470* (1), 53−60.

(2) Badou, A.; Jha, M. K.; Matza, D.; Flavell, R. A. Emerging roles of L-type voltage-gated and other calcium channels in T lymphocytes. *Front. Immunol.* 2013, *4*, 243.

(3) Alves, V. S.; Alves-Silva, H. S.; Orts, D. J. B.; Ribeiro-Silva, L.; Arcisio-Miranda, M.; Oliveira, F. A. Calcium Signaling in Neurons and Glial Cells: Role of Cav1 channels. *Neuroscience* 2019, *421*, 95−111.

(4) D'Ascenzo, M.; Piacentini, R.; Casalbore, P.; Budoni, M.; Pallini, R.; Azzena, G. B.; Grassi, C. Role of L-type Ca2+ channels in neural

stem/progenitor cell differentiation. *Eur. J. Neurosci.* 2006, *23* (4), 935−944.

(5) Eisner, D. A.; Caldwell, J. L.; Kistamas, K.; Trafford, A. W. Calcium and Excitation-Contraction Coupling in the Heart. *Circ. Res.* 2017, *121* (2), 181−195.

(6) Tang, W.; Sencer, S.; Hamilton, S. L. Calmodulin modulation of proteins involved in excitation-contraction coupling. *Front. Biosci.* 2002, *7*, d1583−1589.

(7) Fabiato, A. Calcium-induced release of calcium from the cardiac sarcoplasmic reticulum. *Am. J. Physiol.* 1983, *245* (1), C1−14.

(8) Cens, T.; Rousset, M.; Leyris, J. P.; Fesquet, P.; Charnet, P. Voltage- and calcium-dependent inactivation in high voltage-gated Ca(2+) channels. *Prog. Biophys. Mol. Biol.* 2006, *90* (1−3), 104−117.

(9) Ben-Johny, M.; Yue, D. T. Calmodulin regulation (calmodulation) of voltage-gated calcium channels. *J. Gen. Physiol.* 2014, *143* (6), 679−692.

(10) Sorensen, A. B.; Sondergaard, M. T.; Overgaard, M. T. Calmodulin in a heartbeat. *FEBS J.* 2013, *280* (21), 5511−5532.

(11) Peracchia, C. Calmodulin-Mediated Regulation of Gap Junction Channels. *Int. J. Mol. Sci.* 2020, *21* (2), 485.

(12) Means, A. R.; VanBerkum, M. F.; Bagchi, I.; Lu, K. P.; Rasmussen, C. D. Regulatory functions of calmodulin. *Pharmacol. Ther.* 1991, *50* (2), 255−270.

(13) Wei, J.; Yao, J.; Belke, D.; Guo, W.; Zhong, X.; Sun, B.; Wang, R.; Paul Estillore, J.; Vallmitjana, A.; Benitez, R.; et al. Ca(2+)-CaM Dependent Inactivation of RyR2 Underlies Ca(2+) Alternans in Intact Heart. *Circ. Res.* 2021, *128* (4), e63−e83.

(14) Chin, D.; Means, A. R. Calmodulin: a prototypical calcium sensor. *Trends Cell. Biol.* 2000, *10* (8), 322−328.

(15) Linse, S.; Helmersson, A.; Forsen, S. Calcium binding to calmodulin and its globular domains. *J. Biol. Chem.* 1991, *266* (13), 8050−8054.

(16) Yap, K. L.; Kim, J.; Truong, K.; Sherman, M.; Yuan, T.; Ikura, M. Calmodulin target database. *J. Struct. Funct. Genomics* 2000, *1* (1), 8−14.

(17) Liu, Z.; Vogel, H. J. Structural basis for the regulation of L-type voltage-gated calcium channels: interactions between the N-terminal cytoplasmic domain and Ca(2+)-calmodulin. *Front. Mol. Neurosci.* 2012, *5*, 38.

(18) Black, D. J.; Persechini, A. In calmodulin-IQ domain complexes, the Ca(2+)-free and Ca(2+)-bound forms of the calmodulin C-lobe direct the N-lobe to different binding sites. *Biochemistry* 2011, *50* (46), 10061−10068.

(19) Johny, M. B.; Yang, P. S.; Bazzazi, H.; Yue, D. T. Dynamic switching of calmodulin interactions underlies Ca2+ regulation of CaV1.3 channels. *Nat. Commun.* 2013, *4*, 1717.

(20) Dick, I. E.; Tadross, M. R.; Liang, H.; Tay, L. H.; Yang, W.; Yue, D. T. A modular switch for spatial Ca2+ selectivity in the calmodulin regulation of CaV channels. *Nature* 2008, *451* (7180), 830−834.

(21) Jensen, H. H.; Brohus, M.; Nyegaard, M.; Overgaard, M. T. Human Calmodulin Mutations. *Front. Mol. Neurosci.* 2018, *11*, 396.

(22) Shah, S. R.; Park, K.; Alweis, R. Long QT Syndrome: A Comprehensive Review of the Literature and Current Evidence. *Curr. Probl. Cardiol.* 2019, *44* (3), 92−106.

(23) Liu, N.; Ruan, Y.; Priori, S. G. Catecholaminergic polymorphic ventricular tachycardia. *Prog. Cardiovasc. Dis.* 2008, *51* (1), 23−30.

(24) Landstrom, A. P.; Dobrev, D.; Wehrens, X. H. T. Calcium Signaling and Cardiac Arrhythmias. *Circ. Res.* 2017, *120* (12), 1969−1993.

(25) Limpitikul, W. B.; Dick, I. E.; Joshi-Mukherjee, R.; Overgaard, M. T.; George, A. L., Jr.; Yue, D. T. Calmodulin mutations associated with long QT syndrome prevent inactivation of cardiac L-type Ca(2+) currents and promote proarrhythmic behavior in ventricular myocytes. *J. Mol. Cell. Cardiol.* 2014, *74*, 115−124.

(26) Vassilakopoulou, V.; Calver, B. L.; Thanassoulas, A.; Beck, K.; Hu, H.; Buntwal, L.; Smith, A.; Theodoridou, M.; Kashir, J.; Blayney, L.; et al. Distinctive malfunctions of calmodulin mutations associated

with heart RyR2-mediated arrhythmic disease. *Biochim. Biophys. Acta* **2015**, *1850* (11), 2168−2176.

(27) Crotti, L.; Spazzolini, C.; Tester, D. J.; Ghidoni, A.; Baruteau, A. E.; Beckmann, B. M.; Behr, E. R.; Bennett, J. S.; Bezzina, C. R.; Bhuiyan, Z. A.; et al. Calmodulin mutations and life-threatening cardiac arrhythmias: insights from the International Calmodulinopathy Registry. *Eur. Heart J.* **2019**, *40* (35), 2964−2975.

(28) Chazin, W. J. Relating form and function of EF-hand calcium binding proteins. *Acc. Chem. Res.* **2011**, *44* (3), 171−179.

(29) Bhattacharya, S.; Bunick, C. G.; Chazin, W. J. Target selectivity in EF-hand calcium binding proteins. *Biochim. Biophys. Acta* **2004**, *1742* (1−3), 69−79.

(30) Tidow, H.; Nissen, P. Structural diversity of calmodulin binding to its target sites. *FEBS J.* **2013**, *280* (21), 5551−5565.

(31) Greene, D.; Barton, M.; Luchko, T.; Shiferaw, Y. Computational Analysis of Binding Interactions between the Ryanodine Receptor Type 2 and Calmodulin. *J. Phys. Chem. B* **2021**, *125* (38), 10720−10735.

(32) Halling, D. B.; Georgiou, D. K.; Black, D. J.; Yang, G.; Fallon, J. L.; Quiocho, F. A.; Pedersen, S. E.; Hamilton, S. L. Determinants in CaV1 channels that regulate the Ca2+ sensitivity of bound calmodulin. *J. Biol. Chem.* **2009**, *284* (30), 20041−20051.

(33) Fallon, J. L.; Halling, D. B.; Hamilton, S. L.; Quiocho, F. A. Structure of calmodulin bound to the hydrophobic IQ domain of the cardiac Ca(v)1.2 calcium channel. *Structure* **2005**, *13* (12), 1881−1886.

(34) Webb, B.; Sali, A. Comparative Protein Structure Modeling Using MODELLER. *Curr. Protoc. Bioinformatics* **2016**, *54* DOI: 10.1002/cpbi.3

(35) Van Petegem, F.; Chatelain, F. C.; Minor, D. L., Jr. Insights into voltage-gated calcium channel regulation from the structure of the CaV1.2 IQ domain-Ca2+/calmodulin complex. *Nat. Struct. Mol. Biol.* **2005**, *12* (12), 1108−1115.

(36) Case, D. A.; Cheatham, T. E., 3rd; Darden, T.; Gohlke, H.; Luo, R.; Merz, K. M., Jr.; Onufriev, A.; Simmerling, C.; Wang, B.; Woods, R. J. The Amber biomolecular simulation programs. *J. Comput. Chem.* **2005**, *26* (16), 1668−1688.

(37) Case, D. A.; Aktulga, H. M.; Belfon, K.; Ben-Shalom, I. Y.; Berryman, J. T.; Brozell, S. R.; Cerutti, D. S.; Cheatham, T. E., 3rd; Cisernos, G. A.; Cruzeiro, V. W. D.; et al. *AMBER 22*; University of California: San Francisco, CA, 2023.

(38) Knapp, B.; Ospina, L.; Deane, C. M. Avoiding False Positive Conclusions in Molecular Simulation: The Importance of Replicas. *J. Chem. Theory Comput.* **2018**, *14* (12), 6127−6138.

(39) Roux, B. Continuum Electrostatic Behavior of a 3D-RISM Theory. *J. Phys. Chem. B* **2020**, *124* (34), 7444−7451.

(40) Sengupta, A.; Li, Z.; Song, L. F.; Li, P.; Merz, K. M., Jr. Parameterization of Monovalent Ions for the OPC3, OPC, TIP3P-FB, and TIP4P-FB Water Models. *J. Chem. Inf. Model.* **2021**, *61* (2), 869−880.

(41) Li, Z.; Song, L. F.; Li, P.; Merz, K. M., Jr. Systematic Parametrization of Divalent Metal Ions for the OPC3, OPC, TIP3P-FB, and TIP4P-FB Water Models. *J. Chem. Theory Comput.* **2020**, *16* (7), 4429−4442.

(42) Conde, D.; Garrido, P. F.; Calvelo, M.; Pineiro, A.; Garcia-Fandino, R. Molecular Dynamics Simulations of Transmembrane Cyclic Peptide Nanotubes Using Classical Force Fields, Hydrogen Mass Repartitioning, and Hydrogen Isotope Exchange Methods: A Critical Comparison. *Int. J. Mol. Sci.* **2022**, *23* (6), 3158.

(43) Wang, E.; Sun, H.; Wang, J.; Wang, Z.; Liu, H.; Zhang, J. Z. H.; Hou, T. End-Point Binding Free Energy Calculation with MM/PBSA and MM/GBSA: Strategies and Applications in Drug Design. *Chem. Rev.* **2019**, *119* (16), 9478−9508.

(44) Onufriev, A. V.; Case, D. A. Generalized Born Implicit Solvent Models for Biomolecules. *Annu. Rev. Biophys.* **2019**, *48*, 275−296.

(45) Jeffrey, G. A. *An Introduction to Hydrogen Bonding*; Oxford University Press: Oxford, U.K., 1997.

(46) Roe, D. R.; Cheatham, T. E., 3rd. PTRAJ and CPPTRAJ: Software for Processing and Analysis of Molecular Dynamics Trajectory Data. *J. Chem. Theory Comput.* **2013**, *9* (7), 3084−3095.

(47) Bahler, M.; Rhoads, A. Calmodulin signaling via the IQ motif. *FEBS Lett.* **2002**, *513* (1), 107−113.

(48) Sondergaard, M. T.; Liu, Y.; Larsen, K. T.; Nani, A.; Tian, X.; Holt, C.; Wang, R.; Wimmer, R.; Van Petegem, F.; Fill, M.; et al. The Arrhythmogenic Calmodulin p.Phe142Leu Mutation Impairs C-domain Ca2+ Binding but Not Calmodulin-dependent Inhibition of the Cardiac Ryanodine Receptor. *J. Biol. Chem.* **2017**, *292* (4), 1385−1395.

(49) Wang, K.; Brohus, M.; Holt, C.; Overgaard, M. T.; Wimmer, R.; Van Petegem, F. Arrhythmia mutations in calmodulin can disrupt cooperativity of Ca(2+) binding and cause misfolding. *J. Physiol.* **2020**, *598* (6), 1169−1186.

(50) Prakash, O.; Held, M.; McCormick, L. F.; Gupta, N.; Lian, L. Y.; Antonyuk, S.; Haynes, L. P.; Thomas, N. L.; Helassa, N. CPVT-associated calmodulin variants N53I and A102V dysregulate Ca2+ signalling via different mechanisms. *J. Cell. Sci.* **2022**, *135* (2), 1−15.

(51) Theoharis, N. T.; Sorensen, B. R.; Theisen-Toupal, J.; Shea, M. A. The neuronal voltage-dependent sodium channel type II IQ motif lowers the calcium affinity of the C-domain of calmodulin. *Biochemistry* **2008**, *47* (1), 112−123.

(52) Jensen, H. H; Frantzen, M. T; Wesseltoft, J. L; Busuioc, A.-O.; Møller, K. V; Brohus, M.; Duun, P. R; Nyegaard, M.; Overgaard, M. T; Olsen, A. Human calmodulin mutations cause arrhythmia and affect neuronal function in C. elegans. *Hum. Mol. Genet.* **2023**, *32* (12), 2068−2083.